Energy transformations early in the bacteriorhodopsin photocycle revealed by DNP-enhanced solid-state NMR

Melody L. Mak-Jurkauskas*†, Vikram S. Bajaj†‡§, Melissa K. Hornstein¶‖, Marina Belenky*, Robert G. Griffin†‡, and Judith Herzfeld*,**

*Department of Chemistry, Brandeis University, Waltham, MA 02453; and ‡Department of Chemistry, †Francis Bitter Magnet Laboratory, and ¶Plasma Science and Fusion Center, Massachusetts Institute of Technology, Cambridge, MA 02139

Edited by Ann E. McDermott, Columbia University, New York, NY, and approved December 7, 2007 (received for review July 4, 2007)

By exploiting dynamic nuclear polarization (DNP) at 90 K, we observe the first NMR spectrum of the K intermediate in the ion-motive photocycle of bacteriorhodopsin. The intermediate is identified by its reversion to the resting state of the protein in red light and by its thermal decay to the L intermediate. The ^{15}N chemical shift of the Schiff base in K indicates that contact has been lost with its counterion. Under these circumstances, the visible absorption of K is expected to be more red-shifted than is observed and this suggests torsion around single bonds of the retinylidene chromophore. This is in contrast to the development of a strong counterion interaction and double bond torsion in L. Thus, photon energy is stored in electrostatic modes in K and is transferred to torsional modes in L. This transfer is facilitated by the reduction in bond alternation that occurs with the initial loss of the counterion interaction, and is driven by the attraction of the Schiff base to a new counterion. Nevertheless, the process appears to be difficult, as judged by the multiple L substates, with weaker counterion interactions, that are trapped at lower temperatures. The double-bond torsion ultimately developed in the first half of the photocycle is probably responsible for enforcing vectoriality in the pump by causing a decisive switch in the connectivity of the active site once the Schiff base and its counterion are neutralized by proton transfer.

energy transduction | photocycle intermediates | dynamic nuclear polarization | ion transport | retinal protein

The light-driven ion pump, bacteriorhodopsin (bR), has been studied extensively since it was discovered in the 1970s. Its availability and stability have made it the prototypical transmembrane protein, ion pump, retinal pigment, and model for G protein-coupled receptors. As such, it has been the target of a wide variety of biophysical techniques that have garnered a great deal of information about the structure of the protein and the changes that it undergoes during its functional photocycle. Nevertheless, it remains unclear how the protein stores and channels energy to translocate ions and prevent backflow.

An important feature of the pump cycle (Fig. 1) is that the change in connectivity of the active site between the two sides of the membrane occurs midway through the photocycle (in the transition from the early M state to the late M state), long after the initial photoisomerization of the retinylidene chromophore from *all-trans* to 13-*cis* (Fig. 2), and long before the thermal reisomerization of the chromophore at the end of the photocycle. Because the change in connectivity is divorced from the major isomerization events, much attention has been directed to the process(es) that might be responsible. However, in the fuller context, the more interesting question is how the active site remains connected to the extracellular surface for so long after the photoisomerization event, and what finally releases it from that set of interactions. In this light, it is not surprising that vibrational spectroscopy finds indications of a strained chromophore in the K (1–4) and L (5–8) intermediates, and a relaxed chromophore in the N intermediate (9). Evidence of strain is also seen in magic angle spinning (MAS) NMR spectra. Furthermore, MAS NMR has pinpointed the release of this strain to the transition from early M to late M (i.e., coincident with the connectivity change) and determined that the strain in L and early M is dominated by torsion about double bonds (10, 11). Of course, such torsion is expected to store more energy than torsion about single bonds. In the present work, we examine earlier stages of the photocycle to learn how the torsion seen in the L and early M intermediates develops.

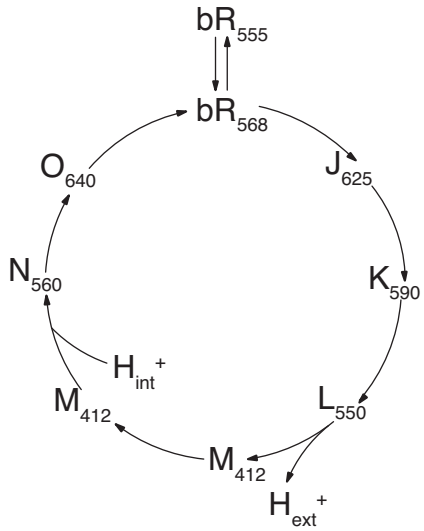

Fig. 1. The ion-motive photocycle of bacteriorhodopsin. The subscript on label for each photocycle intermediate indicates wavelength of maximum visible absorption in nanometers.

NMR has the advantage of providing unique, nonperturbing, site-specific probes that are applicable to mixtures of states, such as are obtained in studies of functional intermediates (12, 13). However, NMR has the disadvantage of low sensitivity, compared with other spectroscopic techniques, because of the small equilibrium polarization of nuclear spins. Recently, dynamic

Author contributions: R.G.G. and J.H. designed research; M.L.M.-J., V.S.B., M.K.H., and M.B. performed research; M.L.M.-J., V.S.B., R.G.G., and J.H. analyzed data; and M.L.M.-J., V.S.B., R.G.G., and J.H. wrote the paper.

The authors declare no conflict of interest.

This article is a PNAS Direct Submission.

§Present address: Department of Chemistry, University of California, Berkeley, CA 94720.

‖Present address: Beam Physics Branch, Plasma Physics Division, Naval Research Laboratory, Washington, DC 20375.

**To whom correspondence should be addressed. E-mail: herzfeld@brandeis.edu.

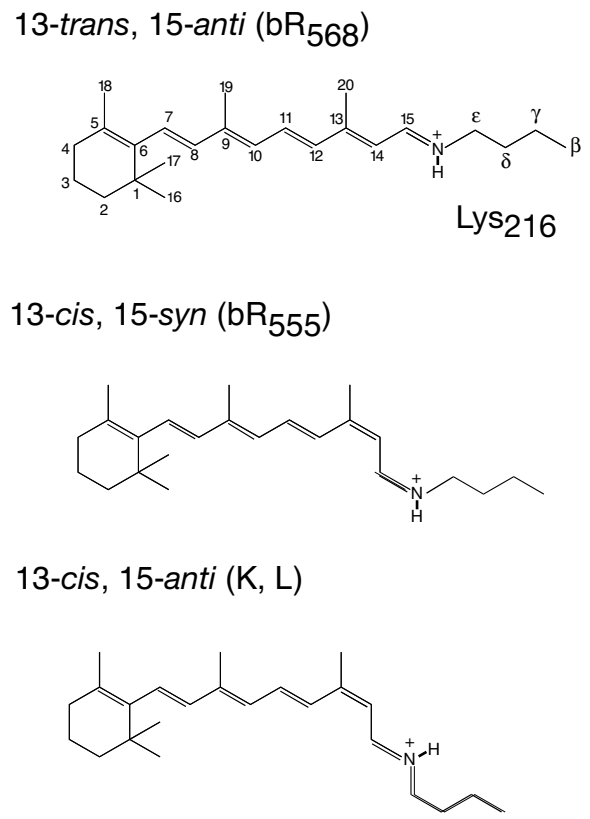

Fig. 2. Retinal configurations in the early photocycle intermediates of bacteriorhodopsin.

nuclear polarization (DNP), in which the greater polarization of electron spins is transferred to the nuclear spins before the NMR experiment (14–16) has been demonstrated to provide large signal enhancements in bacteriorhodopsin in magnetic fields of 5T (17). Here, we apply DNP at 9T, the highest magnetic field at which microwave-driven DNP experiments have been performed to date (18). The experiment requires the application of a continuous microwave field at, or near, the electron resonance frequency and cryogenic temperatures to attenuate spin-lattice relaxation processes that might otherwise compete with polarization transfer. These low temperatures are also useful for trapping the early photocycle intermediates of bR (19). As a result, we have been able to observe the K state by NMR and identify four L substates, three according to their appearance in the thermal relaxation of K and another inferred from changes in signal intensities.

The ^{15}N chemical shift of the Schiff base in these early photocycle intermediates suggests that the mode of energy storage is different in each. By comparison with halide salts of 13-*cis*,15-*anti* retinylidenes and bR variants in which the Schiff base counterion is neutralized, we conclude that the interaction between the chromophore and its counterion is lost in K, but becomes restored and strengthened in L. At the same time, single-bond torsion in the chromophore of the K intermediate is superseded by double-bond torsion in L. These results suggest that photon energy is stored in electrostatic modes in K and is transferred to torsional modes in L. Because release of this torsion has been shown to coincide with the switch in the connectivity of the active site, it is likely responsible for enforcing vectoriality in the pump.

Results

Fig. 3 shows ^{15}N spectra of [ζ-^{15}N]lysine-labeled bR acquired under various conditions. The only significant changes in these spectra, from one case to another, are in the signals from the Schiff base nitrogen of the retinylidene chromophore. These relatively small signals can usually be detected within a few hours because the 40-fold enhancement in sensitivity provided by DNP and low-temperature acquisition.

The spectrum of the dark-adapted sample (Fig. 3*a*) shows bR_{555} and bR_{568} in the expected 60:40 proportion. Subsequent irradiation at 275 K converts bR_{555} to bR_{568} (Fig. 3*b*). The following three spectra (Fig. 3 *c*–*e*) show that different intermediates accumulate depending on the temperature at which the light-adapted bR is irradiated.

Irradiation at 90 K produces two new signals: the larger one upfield of bR_{568} and a smaller one downfield of bR_{568}. Neither of these has previously been detected by NMR. The major product can be assigned to the K state on multiple grounds: first, irradiation with red light results in the expected reversion to bR_{568}; second, as discussed further below, thermal relaxation (in the dark) at 150–170 K gives rise to the observed L photocycle intermediate, confirming that the newly observed species is an intermediate in the functional photocycle. The minor product disappears over a few hours at 90 K. Thus, it appears to be an unstable side-product of the formation of K. According to visible spectroscopy, the generation of K is accompanied by the formation of iso-bR and pseudo-bR, both of which relax to bR_{568} in the dark at 77 K (20). Based on the yields reported in the literature, we tentatively assign the small, most downfield signal in Fig. 3*c* to iso-bR.

At 150 K, the photocycle proceeds beyond the K intermediate, and the L intermediate accumulates. The Schiff base signals observed under these conditions (Fig. 3*d*) reproduce earlier observations (21) but with much improved sensitivity. The most downfield signal was assigned to the L state based on the wavelength dependence of its intensity and on thermal relaxation to the M state. However, for the other signals, it was not possible to exclude contributions from photoproducts of L. In the present work, access to lower temperatures allows us to unambiguously assign all of the signals as substates of L, according to their appearance as products of the thermal relaxation of the K intermediate (about which more below). Furthermore, integration of the spectral intensities in thermal relaxation experiments suggests the presence of yet another L signal within the width of the bR_{568} line at 165 ppm. Thus, we find evidence for four L substates, and distinguish them as L_{165}, L_{174}, L_{181}, and L_{185}, according to their ^{15}N chemical shifts. The inference of multiple, discrete L states is in agreement with recent kinetic analyses of visible (22) spectra and might explain the greater disorder found in x-ray crystallography of the L state at 150 K than at 170 K (23). At the same time, it should be noted that the spectrum in Fig. 3*d* shows no evidence of the K state, although the sample has been cooled to 90 K for data acquisition. This is consistent with recent FTIR studies of cryogenic samples (24). Previous observations of K on cooling L (25) may have been due to irradiation of residual light-adapted bR, whereas in our experiments cooling and data acquisition occur in the dark.

At higher temperatures, the photocycle progresses beyond the L intermediate, and the M intermediate accumulates. The far-downfield signal of the Schiff base (Fig. 3 *e* and *f*) reflects its deprotonated state at this stage of the photocycle. At 210 K, the major product is the early M intermediate, M_o (Fig. 3*e*). Warming to 260 K yields the late M intermediate, M_n (Fig. 3*f*). This also reproduces previously observed behavior (10, 11) and shows that the glycerol content of these samples has not significantly disturbed the progress of the photocycle.

The remaining spectra (Fig. 3 *g*–*i*) show the products of thermal relaxation of the K intermediate at 150 K, 160 K, and 170 K. The fact that all signals produced by red light irradiation at 150 K (Fig. 3*d*) are also produced by thermal relaxation of a single K species at 150 K (Fig. 3*g*) confirms that the signals

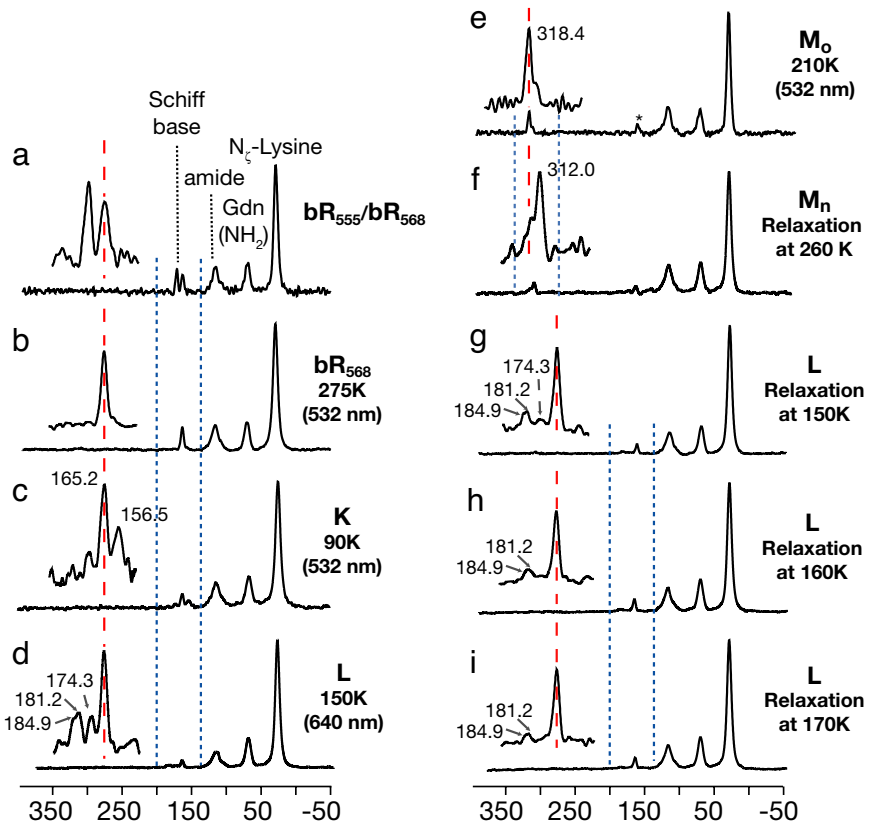

Fig. 3. ^{15}N spectra of photocycle intermediates of [ζ-^{15}N]lysine-bR: (*a*) the dark-adapted state (thermal equilibrium mixture of bR_{555} and bR_{568}); (*b*) the light-adapted state (bR_{568}) accumulated by 532-nm irradiation of *a* at 275 K; (*c*) a mixture of the K intermediate with bR_{568} accumulated by 532-nm irradiation of *b* at 90 K; (*d*) a mixture of L states with bR_{568} accumulated by 640-nm irradiation of *b* at 150 K; (*e*) the early M intermediate accumulated by 532-nm irradiation of *b* at 210 K; (*f*) the late M intermediate accumulated by relaxation of *e* at 260 K; and (*g–i*) the products of the relaxation of *c* at 150 K, 160 K, and 170 K. After accumulation, all intermediates were trapped at 90 K for data acquisition in the dark. (*Insets*) Expansions of the regions between the dashed blue lines. Dashed red lines clarify relationships between the signals.

belong to several L substates. However, at higher temperatures (Fig. 3 *h* and *i*), L_{165}, L_{174}, and L_{181} gradually disappear and we designate the persistent L_{185} as the functional L intermediate. Although it remains to be conclusively determined whether L_{165}, L_{174}, and L_{181}, are precursors of L_{185} or abortive side-products, L_{185} can be identified as the functional, predischarge state, because we observe that it relaxes to M_o on further warming.

In the foregoing spectra, linewidths for the ^{15}N Schiff base resonance are typically 130–170 Hz. Because the chemical shift depends strongly on the electrostatic and electronic environment, these linewidths indicate a well ordered chromophore structure and a distinct environment for each photocycle intermediate.

Chemical shifts for the Schiff bases of each of the 10 species observed in the present work are summarized in Table 1. Most species were generated at least three times to provide a statistical measure of the uncertainty. However, for the less important species, we estimate the accuracy of the Schiff base chemical shifts from an analysis of the resonances of the free lysine side chains in 61 independent ^{15}N spectra of three different samples. These chemical shift deviations were found to follow an approximately normal distribution, with a standard deviation of 0.65 ppm.

Discussion

Dynamic Nuclear Polarization. This work is the first application of DNP to the study of functional intermediates of a protein. With signal enhancements of up to 40-fold, most 1D spectra can be acquired within an hour and longer data acquisition allows the detection of minor components. Despite the necessity of doping with free radicals for DNP, the spectra are of comparable resolution to those obtained in earlier studies at higher temperatures, as long as cryoprotection conditions are adjusted to avoid phase separation of the sample with repeated thermal cycling to liquid nitrogen temperatures. That these conditions are largely compatible with previous protocols for generating and trapping photocycle intermediates is demonstrated by the results in Fig. 3.

Schiff Base–Counterion Interactions. The chemical shift of the Schiff base nitrogen in retinylidenes is extremely sensitive to the interactions of the Schiff base (26–29). In early work on bR, this

Table 1. ^{15}N chemical shifts of the Schiff base in bR

Intermediate	Chemical shift (ppm vs. liquid NH_3)
bR_{555}	173.5 ± 0.65*
bR_{568}	165.2 ± 0.60
Iso-bR	175.4 ± 0.65*
K	156.5 ± 0.72
L_{165} (an unstable L)	165.2 ± 0.60
L_{174} (an unstable L)	174.3 ± 1.02
L_{181} (an unstable L)	181.2 ± 1.2
L_{185} (functional L)	184.9 ± 1.0
M_o (early M)	318.4 ± 0.63
M_n (late M)	312.0 ± 0.65*

*Experimental uncertainty estimated by monitoring lysine resonance at 31.1 ppm.

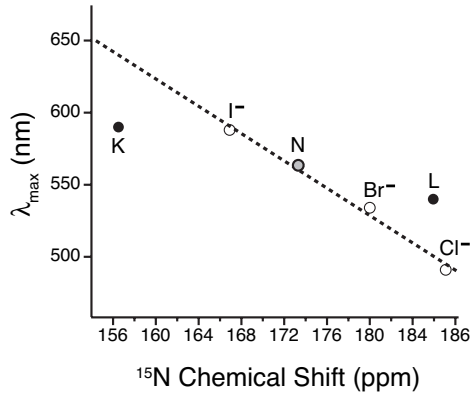

Fig. 4. Relationship between the ^{15}N chemical shifts and the wavelengths of maximum visible absorption in the 13-*cis*,15-*anti* retinylidenes of bacteriorhodopsin (filled circles) and a series of 13-*cis*,15-*anti* retinylidene halides (open circles). The dashed line is a linear fit to the halide series (28). We identify our major, persistent L (L_{185}) with the major, late-L (''L2'') component in time-resolved optical spectra (22).

sensitivity provided evidence for a hydrogen-bonded complex counterion in bR_{568} (27, 30) that was confirmed by x-ray crystallography a decade later (31). It also indicated that the deprotonated Schiff base in each M intermediate has a hydrogen-bonding partner that has not yet been identified (10, 11).

In the present work, we find that the Schiff base signal is far upfield (small chemical shift) in the K intermediate and moves downfield in the L intermediate, as shown along the horizontal axis of Fig. 4. For the latter, we focus on L_{185}, which is the L substate that was previously identified (21), survives at higher temperatures than the others, and thermally relaxes to M_o. Whereas the 185-ppm shift of this persistent L is comparable with that of 13-*cis*,15-*anti* retinylidene chloride, the shift of the K intermediate is so far upfield that it only compares to the shifts of acid blue bR (30) and D85N bR (11) in which the Schiff base counterion has been neutralized by pH titration and mutation, respectively. This suggests that the Schiff base in K has lost contact with the original counterion. Because both D85 and D212 remain unprotonated in K (32) the loss of the counterion interaction must reflect movement in the active site, as expected on isomerization of the chromophore. At the same time, the single narrow NMR signal of the K intermediate indicates a discrete state, in contrast to the considerable disorder seen in NMR spectra of the bR variants with a neutralized counterion. That the counterion interaction is nevertheless severed in K is supported by changes in the C_{15}=N stretch (33) and N–D stretch (34). In addition, polarized FTIR measurements indicate that the N–H bond of the Schiff base is rotated into the plane of the membrane, thereby breaking the hydrogen bond with the counterion complex (34). The highest resolution diffraction structure (35) also shows some rotation of the N–H bond, although not as much as indicated by the polarized FTIR measurements. Narrow NMR lines, indicative of order in the active site, persist through the rearrangements in the L substates that result in reestablishment of counterion interactions. Evidence for a renewed counterion interaction in L has been found in the N–H in-plane bending vibration (3). However, as noted in ref. 21, the chloride-like ^{15}N chemical shift indicates that the counterion interaction in L_{185} is much stronger than the counterion interaction in bR_{568} (which is much weaker even than for the iodide salt). The candidates for such a strong counterion in the active site of L are few: either the Schiff base in L_{185} is approaching one of the two carboxylic acids in the active site more closely than in bR_{568}, or water hydrogen bonded to the Schiff base is becoming highly polarized. A direct interaction with water is supported by FTIR observations of coupling between water and the C_{15}-HOOP and N-HOOP modes of the chromophore in L (36). The highest-resolution diffraction structure also shows water intervening between the Schiff base and D85 (37). The NMR evidence that such a water molecule must be highly polarized has motivated speculation that bR may be acting as an inward-driven hydroxyl pump rather than an outward-driven proton pump (12, 13).

Polyene Torsion. The interactions of the Schiff base affect not only the chemical shift of the nitrogen, but also the visible spectrum of the chromophore. For a given configuration of the retinylidene, the relationship between the ^{15}N chemical shift and the frequency of maximum visible absorption is linear (28–30). This is illustrated in Fig. 4 for a set of halide salts of 13-*cis*,15-*anti* retinylidenes. In this series, the only variation from one model compound to the other is the counterion. Comparison with the data for the 13-*cis*,15-*anti* intermediates of the bR photocycle (also shown in Fig. 4) must take into account other influences on the visible spectrum, particularly strain in the polyene chain. Distortion involving rotations about single bonds gives rise to wavelengths of maximum visible absorption that are shorter than expected based on the ^{15}N chemical shift; conversely, distortion involving torsion about double bonds yields wavelengths of maximum visible absorption that are longer than expected based on the ^{15}N chemical shift (38). These relationships were the basis of previous conclusions that the change in connectivity in the active site coincides with a release of double-bond torsion in the chromophore (11).

Here, we extend this analysis to earlier stages of the photocycle, identifying our persistent L (L_{185}) with the late-L (''L2'') characterized by decomposition of time-resolved optical spectra (22). As shown in Fig. 4, the K intermediate is blue-shifted relative to expectations based on its Schiff base environment (i.e., not as red-shifted as expected), whereas the L intermediate is red-shifted relative to expectations based on its Schiff base environment. This suggests that chromophore strain in the K intermediate is primarily about single bonds, whereas chromophore strain in the L intermediate appears to be primarily about double bonds. Such double-bond torsion stores more energy and is presumably compensated by reestablishment of a counterion interaction.

The analysis above only illuminates the relative contributions of single- and double-bond torsion. However, C_{15}-HOOP signals in K (1–4) and L (6–8) suggest that the locus of the distortion is at C_{15} in both intermediates and, therefore, that the single-bond torsion in K is primarily around the C_{14}–C_{15} bond and the double-bond torsion in L is primarily around the C_{15}=N bond. In any case, the results are difficult to reconcile with crystal structures. Although the models for K and L based on the highest-resolution diffraction data have highly distorted chromophores, the torsion in both cases is primarily in the C_{13}=C_{14} and C_{15}=N bonds (35, 37).

Energy Landscape. The present overall picture is one of initial storage of energy in breaking the Schiff base–counterion interaction, with relatively little energy stored in polyene torsion, followed by stronger twisting of the chromophore, under the influence of new counterion interactions. This transfer of energy from electrostatic modes to torsional modes would be facilitated by the reduction of bond order alternation in the polyene (corresponding to delocalization of the retinylidene charge) when the counterion interaction is initially broken, and would be driven by the establishment of a new counterion interaction.

Of the 216 kJ/mol carried by 568-nm-wavelength photons, the K state is thought to store 45 kJ/mol (39). Because hydrogen bond strengths vary over 5–40 kJ/mol, breaking an exceptionally strong hydrogen bond in the transition from bR_{568} to K can store essentially all of the required energy, with possible further contributions from perturbation of other hydrogen bonds. Although it is often noted that the Schiff base–counterion inter-

action in bR_{568} is weak, this is relative to the retinylidene halide salts. In bR_{568}, the interaction of the Schiff base with the anions in the active site is indirect and mediated by water. Thus, a strong hydrogen bond to water in bR_{568} is consistent with an overall weak counterion interaction.

The NMR results also reveal that the process of converting the electrostatic energy stored in K to torsion energy stored in L_{185} is a difficult one. Although the ^{15}N chemical shifts indicate that the Schiff bases of all of the L substates have renewed counterion interactions, the interactions are weaker in the less stable L states than in persistent L_{185}. Unfortunately, without visible absorption information or more detailed NMR experiments, we have no insight into chromophore torsion in these species. Moreover, the present NMR spectra do not allow us to determine whether the less stable L states relax to the functional L_{185} state or short-circuit back to the bR_{568} state. However, whether these states represent hesitant steps on the functional pathway or missteps off the pathway, they clearly reflect a rugged energy landscape. Such a landscape is consistent with recent quantum mechanical/molecular mechanical calculations that find two plausible L states that differ substantially in chromophore torsion and in Schiff base interactions (40). Two discrete L states have also been inferred from analyses of visible spectra (22). However, the present NMR study finds that K thermally relaxes to at least four distinct and directly observable states.

Conclusions

DNP-enhanced solid-state NMR spectroscopy at cryogenic temperatures has provided the first NMR observation of the K intermediate of the ion-motive photocycle of bR, and afforded firm identification of the NMR signals of several L intermediates. The ^{15}N chemical shifts of the chromophores of these species indicate that the Schiff base loses contact with its counterion in K and establishes a new counterion interaction in L. At the same time, low-energy, single-bond torsion in K evolves to high-energy, double-bond torsion in the functional L state. Thus, photon energy initially stored in electrostatic form is transformed to torsion that is probably responsible for the decisive switch in the connectivity of the active site when the Schiff base and its counterion are neutralized by proton transfer. Such a switch is critical for preventing backflow in the pump. Clarification of the roles of the less stable L states is underway by multidimensional spectroscopy. However, their presence indicates that the reorganization of the active site in the K-to-L transition involves passage over an energy landscape riddled with traps and/or detours.

Materials and Methods

Sample Preparation. [ζ-^{15}N]lysine-labeled bR was prepared by growing *Halobacterium salinarium* strain (JW-3) in a synthetic medium containing L-[ζ-^{15}N]lysine (41). The purple membrane, isolated and purified according to the method of Oesterhelt and Stoeckenius (42), was washed in 0.3 M guanidinium hydrochloride at pH 10, until the supernatant had the same pH, and then washed further with 60% glycerol (vol/vol, for cryoprotection) (43) containing 0.3 M guanidinium hydrochloride, and 40 mM 4-amino 2,2,6,6-tetramethylpiperidine-*N*-oxyl (TEMPO) [the exogenous nitroxide radical required for the DNP experiments (17, 44)], at pH 10. The washed purple membrane was collected in a pellet by ultracentrifugation (1 h at 323,000 $\times$ *g*) and packed into the center of a 4-mm-diameter, single-crystal sapphire rotor that is transparent at both optical and millimeter-wave frequencies. The drive tip was bonded to the sapphire rotor by using a low-temperature epoxy to avoid problems associated with thermal contraction at cryogenic temperatures. The sample was reversibly sealed by using a vespel screw that threads into a Kel-F top spacer with a diameter such that it must be inserted under liquid nitrogen. The total sample volume was 57 μl.

Preparation of Photocycle Intermediates. To generate photocycle intermediates, light was delivered to the sample by using a multimode fiber that penetrates the MAS stator housing perpendicular to the rotor and projects a diffuse beam of diameter comparable to the sample size. The light sources were a 300-mW diode-pumped solid-state laser (Coherent) operating at 532 nm (green), and a krypton laser (Cambridge Laser Laboratories) producing 1 W at 647 nm (red). Each photocycle intermediate was accumulated at the temperature that maximizes its yield relative to other states and then cooled (3–5 K/min) to 90 K to trap the intermediate for data acquisition. Operation of either light source raised the sample temperature by <0.5 K.

bR_{568}. bR_{568} (the ''light-adapted'' state), was generated by irradiation of the dark-adapted sample (a mixture of bR_{568} and bR_{555} at thermal equilibrium) with green light for 45 min at 278 K.

K. K was generated by irradiation of bR_{568} at 90 K with green light for 45 min.

L. L was prepared by thermal relaxation of the K intermediate, at 150, 160, or 170 K, and also by irradiation of bR_{568} for 4 h at 150 K with red light.

M_o and M_n. The early M intermediate (M_o) was prepared by irradiation of bR_{568} with green light at 210 K for 45 min. The late M intermediate (M_n) was prepared by thermal relaxation of early M at 260 K.

To avoid interference with the generation of photocycle intermediates, weak IR light was used to monitor the MAS spinning frequency.

DNP/NMR Spectroscopy. All experiments were carried out at 9T by using the 250 GHz e^-/380 MHz ^1H DNP spectrometer with a three radiofrequency channel (^1H, ^{13}C, ^{15}N) probe that incorporates matching transmission lines to provide remote tuning, high isolation between the channels, and high radiofrequency stability with respect to temperature variations in the sample chamber (45). The NMR spectrometer console was designed and built in-house and uses custom-designed NMR data acquisition software (D. J. Ruben, Francis Bitter Magnet Laboratory, MIT).

Millimeter-wave power is produced by a 250-GHz gyrotron oscillator (45, 46). The beam is directed to the sample through a quasi-optical transmission circuit consisting of two HE_{11}-mode overmoded corrugated waveguides and an optical matching circuit between them (18, 47). Gaussian mode purity is maintained throughout the transmission system, resulting in negligible transmission losses, and 2–4 W of microwave power are delivered to the sample. The transmission circuit incorporates a quasi-optical beam splitter for feedback regulation of the microwave power. A computer control system guarantees safe and unattended operation of the device with power stability of $>1\%$.

One-dimensional NMR spectra were recorded by using ramped cross-polarization (48, 49) with high-power proton decoupling and MAS for high resolution (50, 51). Typically, the cross-polarization involved a ^1H field of 45 kHz, with the ^{13}C or ^{15}N power ramped linearly over the $n = 1$ matching condition. Data were acquired with optimized two-pulse phase modulation (TPPM) (52), decoupling at 100-kHz field strength, and magic angle spinning at a frequency of 6.25–6.5 kHz.

Cryogenic MAS was accomplished through the use of bearing-and-drive nitrogen gas streams that have been cooled by using a pressurized heat exchanger immersed in liquid nitrogen. The gas transfer lines incorporate integral heaters and calibrated resistive temperature sensors for feedback regulation of the temperature (LakeShore Cryotronics). However, the temperatures that we report are measured in the sample chamber by using a Fabry–Perot interferometric thermometer (FISO Technologies), which is insensitive to magnetic and radiofrequency fields and is accurate to within 1 K. The spinning frequency was regulated to within 2–3 Hz by a pneumatic controller (Bruker Biospin).

All ^{15}N chemical shifts are referenced indirectly to liquid ammonia by using adamantane as an external standard and following the procedure of Morcombe and Zilm (53). Because of the temperature dependence of the chemical shift, which can arise due to intrinsic and extrinsic (instrument-related) factors, we have referenced all spectra by using the chemical shift of adamantane at the temperature of acquisition (usually 90 K).

ACKNOWLEDGMENTS. We thank Ajay Thakkar, Peter Allen, Jeffrey Bryant, David J. Ruben, Paul P. Woskov, Jagadishwar R. Sirigiri, and Christopher J. Turner for technical assistance. This work was supported by National Institutes of Health Grants EB001035, EB001960, EB002026, and EB004866 and by a postgraduate fellowship from the Natural Sciences and Engineering Research Council of Canada (to V.S.B.).

1. Braiman M, Mathies R (1982) *Proc Natl Acad Sci USA* 79:403–407.
2. Gat Y, Grossjean M, Pinevsky I, Takei H, Rothman Z, Sigrist H, Lewis A, Sheves M (1992) *Proc Natl Acad Sci USA* 89:2434–2438.
3. Maeda A, Sasaki J, Pfefferle JM, Shichida Y, Yoshizawa T (1991) *Photochem Photobiol* 54:911–921.
4. Weidlich O, Ujj L, Jager F, Atkinson GH (1997) *Biophys J* 72:2329–2341.

5. Argade PV, Rothschild KJ (1983) *Biochemistry* 22:3460–3466.
6. Diller R, Stockburger M, Oesterhelt D, Tittor J (1987) *FEBS Lett* 217:297–304.
7. Fahmy K, Siebert F, Grossjean MF, Tavan P (1989) *J Mol Struct* 214:257–288.
8. Weidlich O, Siebert F (1993) *Appl Spectrosc* 47:1394–1400.
9. Yamazaki Y, Kandori H, Needleman R, Lanyi JK, Maeda A (1998) *Biochemistry* 37:1559–1564.
10. Hu JG, Sun BQ, Bizounok M, Hatcher ME, Lansing JC, Raap J, Verdegem PJE, Lugtenburg J, Griffin RG, Herzfeld J (1998) *Biochemistry* 37:8088–8096.
11. Hatcher ME, Hu JG, Belenky M, Verdegem P, Lugtenburg J, Griffin RG, Herzfeld J (2002) *Biophys J* 82:1017–1029.
12. Herzfeld J, Lansing JC (2002) *Annu Rev Biophys Biomol Struct* 31:73–95.
13. Herzfeld J, Tounge B (2000) *Biochim Biophys Acta Bioenerg* 1460:95–105.
14. Abragam A, Proctor WG (1958) *Compt Rend* 246:2253–2256.
15. Wind RA, Duijvestijn, MJ, van der Lugt C, Manenschijn A, Vriend J (1985) *Prog NMR Spectrosc* 17:33–57.
16. Goldman M (1970) *Spin Temperature and Nuclear Magnetic Resonance in Solids* (Clarendon Press, Oxford).
17. Rosay M, Lansing JC, Haddad KC, Bachovchin WW, Herzfeld J, Temkin RJ, Griffin RG (2003) *J Am Chem Soc* 125:13626–13627.
18. Bajaj VS, Farrar CT, Mastovsky I, Vieregg J, Bryant J, Elena B, Kreischer KE, Temkin RJ, Griffin RG (2003) *J Magn Reson* 160:85–90.
19. Balashov SP, Ebrey TG (2001) *Photochem Photobiol* 73:453–462.
20. Balashov SP (1995) *Isr J Chem* 35:415–428.
21. Hu JG, Sun BQ, Petkova AT, Griffin RG, Herzfeld J (1997) *Biochemistry* 36:9316–9322.
22. Zimanyi L, Saltiel J, Brown LS, Lanyi JK (2006) *J Phys Chem A* 110:2318–2320.
23. Lanyi JK, Schobert B (2003) *J Mol Biol* 328:439–450.
24. Dioumaev AK, Lanyi JK (2007) *Proc Natl Acad Sci USA* 104:9621–9626.
25. Kouyama T, Nishikawa T, Tokuhisa T, Okumura H (2004) *J Mol Biol* 335:531–546.
26. Harbison GS, Herzfeld J, Griffin RG (1983) *Biochemistry* 22:1–5.
27. de Groot HJM, Harbison GS, Herzfeld J, Griffin RG (1989) *Biochemistry* 28:3346–3353.
28. Hu JG, Griffin RG, Herzfeld J (1994) *Proc Natl Acad Sci USA* 91:8880–8884.
29. Hu JGG, Griffin RG, Herzfeld J (1997) *J Am Chem Soc* 119:9495–9498.
30. de Groot HJM, Smith SO, Courtin J, Vandenberg E, Winkel C, Lugtenburg J, Griffin RG, Herzfeld J (1990) *Biochemistry* 29:6873–6883.
31. Luecke H, Schobert B, Richter HT, Cartailler JP, Lanyi JK (1999) *J Mol Biol* 291:899–911.
32. Braiman MS, Mogi T, Marti T, Stern LJ, Khorana HG, Rothschild KJ (1988) *Biochemistry* 27:8516–8520.
33. Rothschild KJ, Roepe P, Lugtenburg J, Pardoen JA (1984) *Biochemistry* 23:6103–6109.
34. Kandori H, Belenky M, Herzfeld J (2002) *Biochemistry* 41:6026–6031.
35. Schobert B, Cupp-Vickery J, Hornak V, Smith SO, Lanyi JK (2002) *J Mol Biol* 321:715–726.
36. Maeda A, Balashov SP, Lugtenburg J, Verhoeven MA, Herzfeld J, Belenky M, Gennis RB, Tomson FL, Ebrey TG (2002) *Biochemistry* 41:3803–3809.
37. Lanyi JK, Schobert B (2007) *J Mol Biol* 365:1379–1392.
38. Kropf A, Hubbard R (1959) *Ann N Y Acad Sci* 74:266–280.
39. Birge RR, Cooper TM, Lawrence AF, Masthay MB, Zhang CF, Zidovetzki R (1991) *J Am Chem Soc* 113:4327–4328.
40. Bondar AN, Elstner M, Suhai S, Smith JC, Fischer S (2004) *Structure (London)* 12:1281–1288.
41. Argade PV, Rothschild KJ, Kawamoto AH, Herzfeld J, Herlihy WC (1981) *Proc Natl Acad Sci USA* 78:1643–1646.
42. Oesterhelt D, Stoeckenius W (1973) *Proc Natl Acad Sci USA* 70:2853–2857.
43. Kalisky O, Ottolenghi M, Honig B, Korenstein R (1981) *Biochemistry* 20:649–655.
44. Gerfen GJ, Becerra LR, Hall DA, Griffin RG, Temkin RJ, Singel DJ (1995) *J Chem Phys* 102:9494–9497.
45. Bajaj VS, Hornstein MK, Kreischer KE, Sirigiri JR, Woskov P, Mak-Jurkauskas ML, Herzfeld J, Temkin RJ, Griffin RG (2007) *J Magn Reson* 189:251–279.
46. Kreischer KE, Farrar C, Griffin R, Temkin R, Vieregg J (2000) in *ICOPS 2000. IEEE Conference Record–Abstracts. 27th IEEE International Conference on Plasma Science* (IEEE, Piscataway NJ), p 198.
47. Woskov PP, Bajaj VS, Hornstein MK, Temkin RJ, Griffin RG (2005) *IEEE Trans Microw Theory Tech* 53:1863–1869.
48. Pines A, Gibby MG, Waugh JS (1973) *J Chem Phys* 59:569–590.
49. Hediger S, Meier BH, Kurur ND, Bodenhausen G, Ernst RR (1994) *Chem Phys Lett* 223:283–288.
50. Andrew ER, Bradbury A, Eades RG (1958) *Nature* 182:1659.
51. Lowe IJ (1959) *Phys Rev Lett* 2:285–287.
52. Bennett AE, Rienstra CM, Auger M, Lakshmi KV, Griffin RG (1995) *J Chem Phys* 103:6951–6958.
53. Morcombe CR, Zilm KW (2003) *J Magn Reson* 162:479–486.